Electronic Supplementary Information

Solution processed large area fabrication of Ag patterns as electrodes for flexible heaters, electrochromics and organic solar cells

By *Ritu Gupta,*[a] *Sunil Walia,*[a] *Markus Hösel,*[b] *Jacob Jensen,*[b] *Dechan Angmo,*[b] *Frederik C. Krebs*[b] * *and Giridhar U. Kulkarni*[a] *

[a][*] Prof. Giridhar U. Kulkarni, Ritu Gupta and Sunil Walia
Chemistry and Physics of Materials Unit,
DST Unit on Nanoscience,
Jawaharlal Nehru Centre for Advanced Scientific Research,
Jakkur P.O., Bangalore, India-560064
Email: kulkarni@jncasr.ac.in

[b][*] Prof. Frederik C. Krebs, Markus Hösel, Jacob Jensen, and Dechan Angmo
Department of Energy Conversion and Storage, Technical University of Denmark,
Frederiksborgvej 399, DK-4000 Roskilde, Denmark
Email: frkr@dtu.dk

Table S1 summarizes literature on usage of commercial laser printers for different applications.

S.No.	Printer Model	Resolution (DPI)	Device minimum feature size (µm)	Substrate	Application	Reference
1.	Laser Plotter RG 8500	25400	4	photomask film	micropatterning of biomaterials	Lab Chip, 2009, 9 (1), 167-70
2.	*HP* LaserJet P2015dn	1200	70	Kapton sheet	micropatterned CNTs growth	ACS Appl. Mater. & Interf. 2013, 5, 3656
3.	HP model 1102w	1200	100	polyester film	Clinical diagnostics	Anal. Chem. 2012, 84 (21), 9002-7
4.	Samsung ML-2250	1200	200	Copper sheet	Digital microfluidics	Adv. Mater. 2007, 19 (1), 133-137
5.	Laser Printer EPL 5800	1200	200	PET	microfluidic devices	Lab Chip 2005, 5 (9), 974-8
6.	HP Color LaserJet 4700 dn	600	100	PET	DNA chips	RSC Adv. 2012, 2 (6), 2308
7.	laser-printer --	600	200	PET	prototyping of microchannels	Lab Chip 2007, 7 (7), 931-4
8.	HP LaserJet 4M	1200	100	PET	LED display	Adv. Funct. Mater. 2005, 15 (1), 51-56
9.	**Ricoh 5000**	**1200**	**150**	**Kapton, PET, Scotch tape, thermal tape, mica, paper**	**electrochromic, microheaters,OPV**	**Present Study**

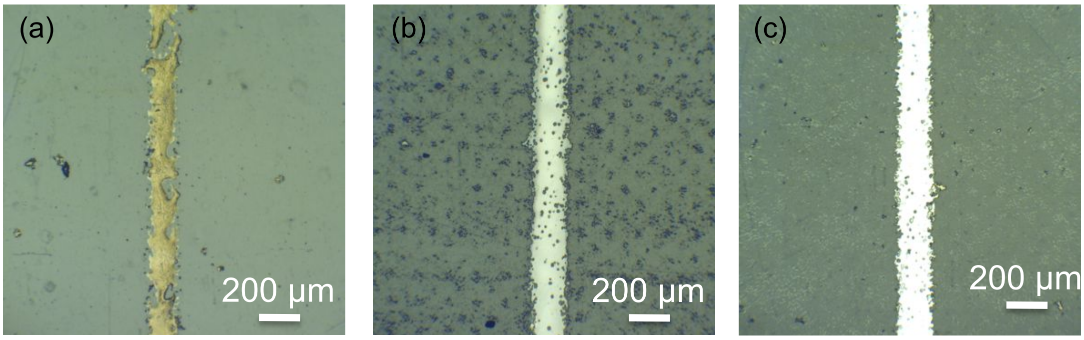

Fig. S1 Ag inks of different type (a) Nanoparticle based Ag ink (Paru PI-015) and non-particle based inks (b, c) from Kunshan Hisense (SC-100) and Inktec (PR-010) respectively.

As seen from the Fig. S1, non-particle based Ag ink (Fig. S1b and c) give better results than nanoparticle based Ag ink (Fig. S1a). The nanoparticle based Ag ink has highly non-uniform thickness and comes-off from the patterned regions during lift-off process, whereas the adhesion of non-particle based ink is almost unaffected by any mechanical treatment. The non-particle Ag inks in Fig. S1b and c showed well-defined edges. Inktec Ag ink was chosen instead of Hisense ink due to its excellent adhesion with the PET resulting in clean removal of toner during lift-off.

	Supplier	Ink Type	Ag wt%	Resistivity (µΩ-cm)	For Product details:
1	PARU (PI-015)	Nanoparticle based (~50 nm)	20	8	http://www.fonton.com/en/product-inner.php?id=151
2	Kunshan Hisense (SC100)	Non-particle	20	5	http://en.kshisense.com/products_detail/&productId=7619c268-b560-43c5-8813-46ee9c2f98e8&comp_stats=comp-FrontProducts_list01-dddesx8807043.html
3	Inktec (PR010)	Non-particle	10	5	http://www.inktec.com/english/distributor/where_write_ko.asp?product_flag=Electronic

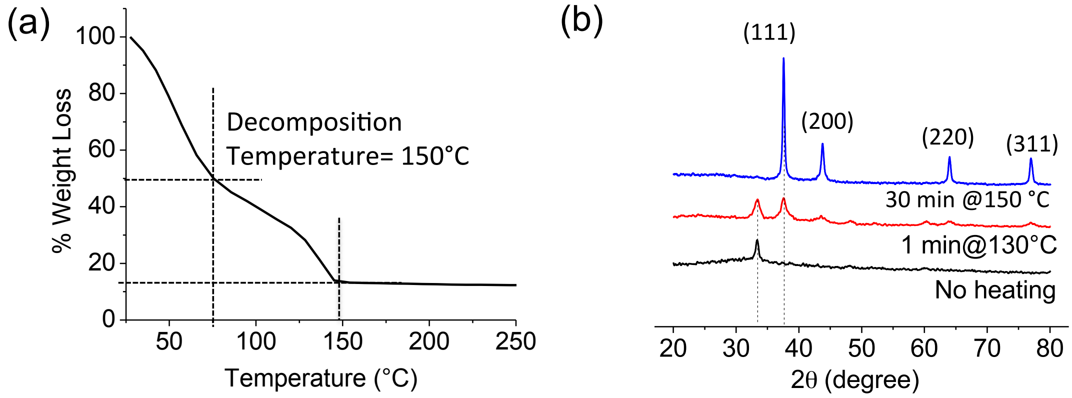

Fig. S2 (a) Thermogravimetric analysis of Ag precursor ink at a scan rate of 10 °C/min (b) XRD pattern of Ag ink before and after heating.

The thermo gravimetric analysis (TGA) data exhibits a weight loss of 88 % on Ag formation at relatively lower temperature of 150 °C (see Fig. S2a). The formation of Ag is confirmed by studying the X ray diffraction pattern of Ag precursor ink before and after treatment. One can clearly see the appearance of sharp peaks characteristic of Ag. The XRD pattern of the Ag ink before and after decomposition is shown in Fig. S2b that shows complete formation of crystalline FCC Ag.

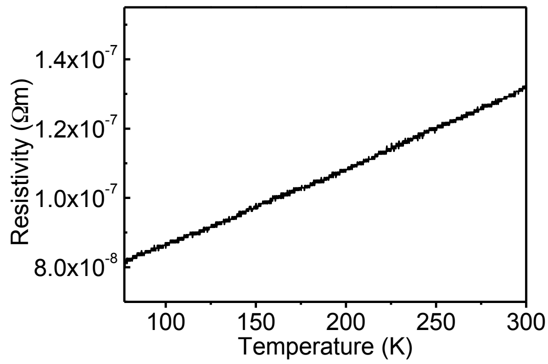

Fig. S3 Temperature dependent resistivity of the Ag film.

The 4-probe resistance of the Ag film was measured while cooling from 300K to 50K at 10 °C/min. The electrical resistivity at 300K was calculated to be 1.31×10^{-7} Ω.m, which is 8.23 times higher than the bulk value. The higher value can be due to the presence of carbon impurities. From the temperature dependent data, a TCR value of 1.75×10^{-3} K^{-1} was estimated, which is 3.5 times lower than the bulk value of 6.1×10^{-3} K^{-1}. Lower TCRs values are common to any metal films containing some disorder.

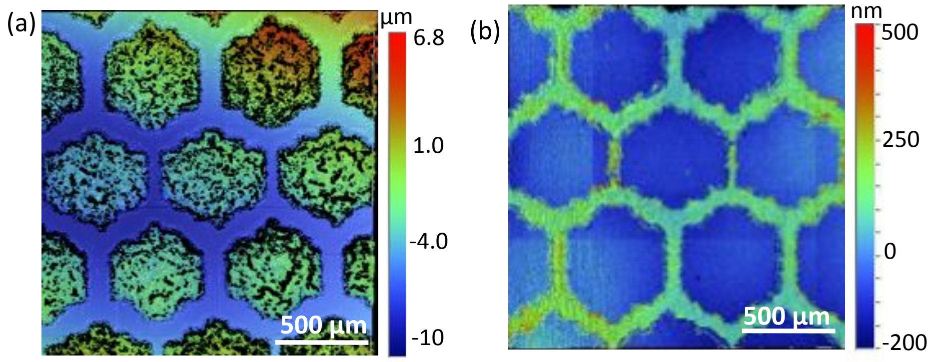

Fig. S4 Optical Profilometric Image of (a) Toner/PET and (b) Ag PET after developing with Ag and removal of toner.

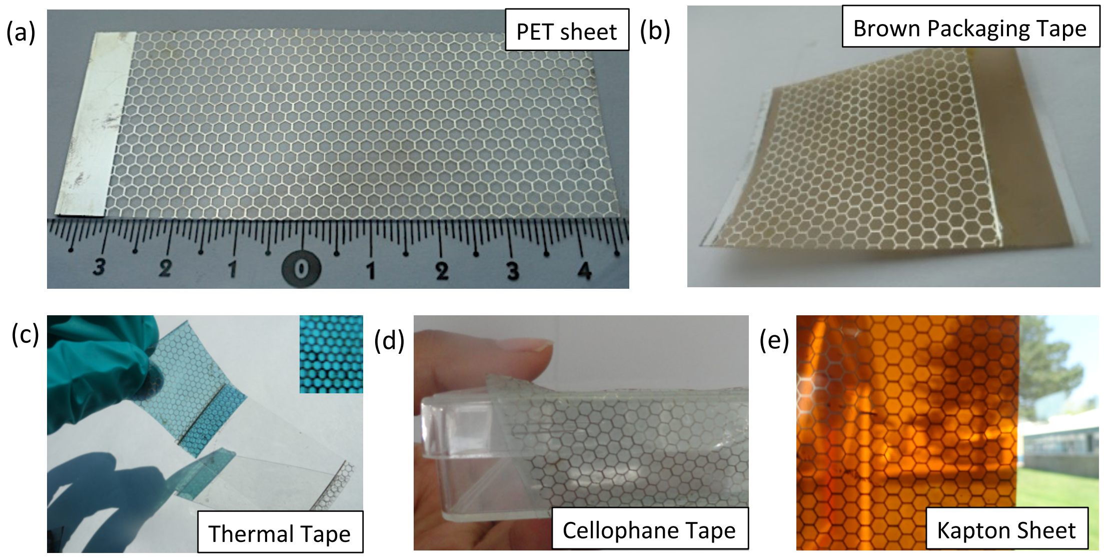

Fig. S5 Ag pattern printed on various substrates (a) PET sheet (b) brown packaging tape (c) thermal Tape (d) clear cellophane tape and (e) polyimide

The different substrates are pasted on PET substrate for printing with laser printer. The substrates are treated with UV-plasma for modifying the surface properties of different substrate and improving the adhesion of Ag.

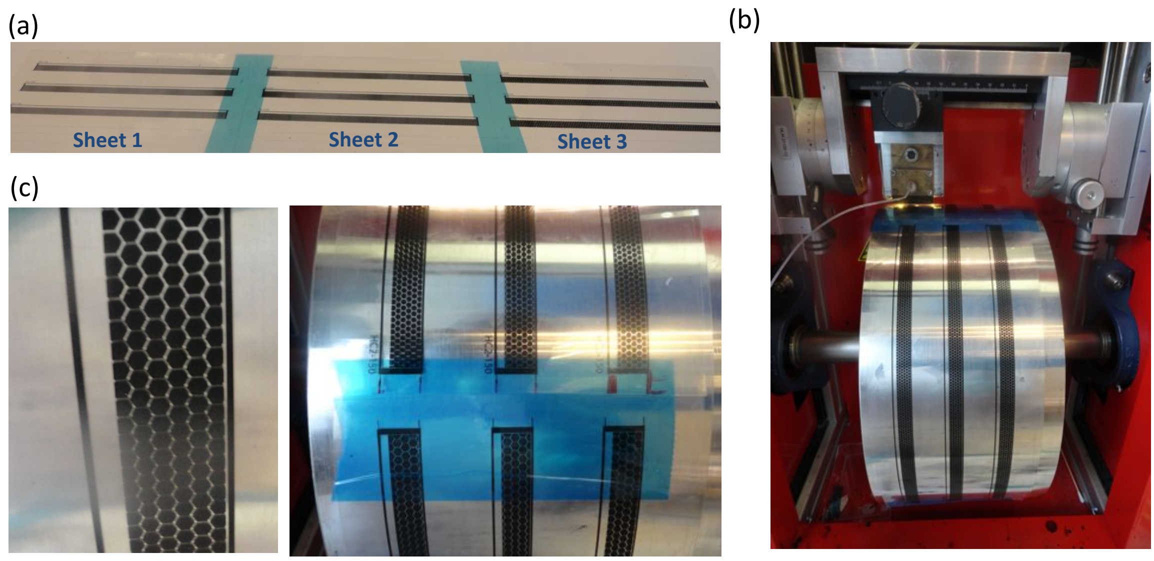

Fig. S6 Printing of large area A4 size patterns for roll coater (a) A4 size sheets printed in toner using office laser printer are converted to a 1 m roll by pasting together using thermal tape. (b) toner printed sheets mounted on roll coater prior to Ag ink deposition.

The printing method could also be extended to large area coating using a slot die head roll coater. The toner printed sheets of A4 size with hexagonal patterned grids were joined together to form 1 m length (Fig. S6). The extended sheet was mounted on a motorized roll of 300 mm diameter and aligned with the help of markers shown in Fig. S6c.

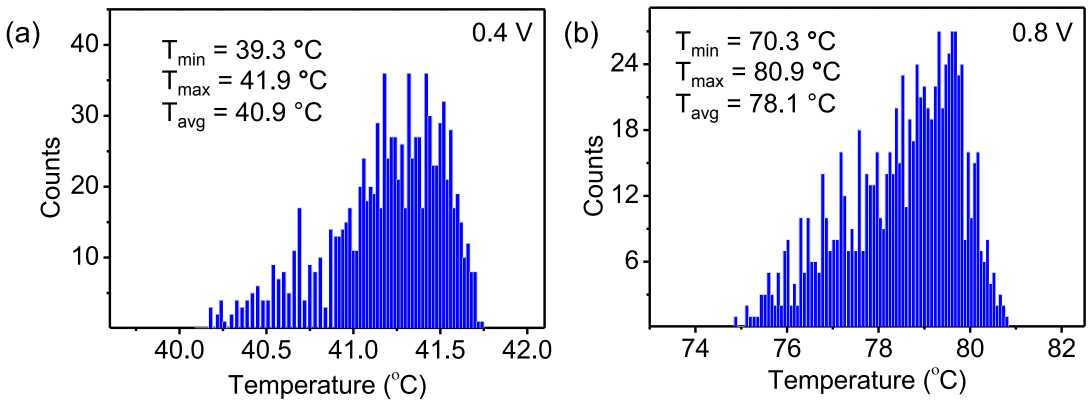

Fig. S7 Histograms showing the average temperature distribution across the sample area corresponding to thermal images acquired for the line heater in Fig. 4 at (a) 0.4 V and (b) 0.8 V.

Table S2 Change in resistance after heating cycles at different voltages.

	Voltage (V)	Current (mA)	Time (min)	T_{avg} (^oC)	$R_{s,initial}$ (Ω)	$R_{s,final}$ (Ω)	$\Delta R/R\times100$ (%)
1	0.2	86.08	2	25	2.328	2.331	0.12
2	0.3	129.12	2	30	2.331	2.325	0.25
3	0.5	212.59	2	45	2.325	2.326	-0.04
4	0.8	328.45	2	70	2.326	2.335	0.38
5	1.25	504.11	2	125	2.335	2.249	-3.68

The change in resistance during heating cycles at different applied voltages (after 2 min) is shown in the table below. The resistance change is notably small at lower voltages. At a voltage of 1.25 V, the heater attains temperature of 125 ^oC, decreasing the resistance by 3.68%, due to annealing.

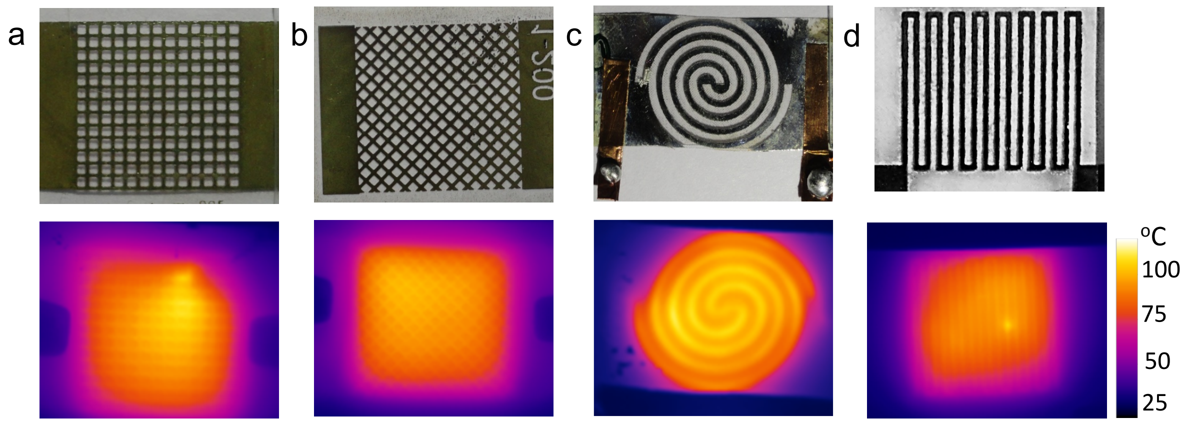

Fig. S8 Various heater designs (a) square mesh (b) pyramid shape (c) spiral and (d) zig-zag path.

Since the technique is versatile, different designs of heaters were printed. Depending on the resistance of individual design, the constant voltage was applied to raise the temperature to approximately between 90 – 110 °C which PET can sustain. As seen from Fig. S8(a and b), the grids are interconnected and posses resistance as low as 2 Ω. In this case, a constant voltage of 1.4 V is applied to raise the temperature. The spiral (Fig. S8c) and zig-zag design (Fig. S8d) run continuously over longer path thus exhibiting higher resistance of 64 Ω and 126 Ω respectively. Due to the higher resistance, spiral pattern required 3 V to reach the temperature of 90 -110 °C whereas a much higher voltage of 7 V was applied for zigzag pattern.

Table S3 A brief survey of literature transparent microheaters.

S. NO	Types of heater	Synthesis Solution/Physical	Area (cm^2)	Voltage (V)	Max Temp (^oC)	Resistance (Ω sq. $^{-1}$)	Transparency (%)	Reference
1	MWCNT	CVD	0.65 × 0.85	15	77	699	83	Carbon 2011, 49 (1), 111-116
2	SWCNT	Arc discharge	4 × 4	12	100	580	79	Adv. Mater. 2007, 19 (23), 4284-4287
3	SWCNT	Arc discharge	1 × 1	60	47	20600	95	Carbon 2011, 49 (4), 1087-1093
4	Silver Nanowires	Solution based	2.5 × 2.5	7	53	33	90	Nano Res. 2012, 5 (6), 427-433
5	ITO NPs film	Solution based	~ 2 × 2	50	180	-	90	J. Nanosci. Nanotech. 2013, 13 (5), 3519-3521
6	Silver Nanowires	Solution based	2.5 × 2.5	7	100	10	90	Adv. Funct. Mater. 2013, 23 (10), 1250-1255
7	CVD Graphene	CVD	2 × 2	40	80	750	85	Current Appl. Phys. 2012, 12, S113-S117
8.	R- GO	Solution based	2 × 1.4	60	206	641	34	Small 2011, 7 (22), 3186-92
9.	Doped Graphene	CVD	4 × 4	12	100	43	89	Nano lett. 2011, 11 (12), 5154-8
10.	Doped Graphene	CVD	2 × 2	12	110	66	90	Adv. Funct. Mater. 2012, 22 (22), 4819-4826
11	CNTs& Ag nanowires	Solution based	4 × 4	15	110	~ 50	~ 85-95	Carbon 2013, 63 (0), 530-536
12.	**Ag patterns**	**Solution based**	**1 × 1**	**1**	**120**	**2**	**60-80**	**Present study**

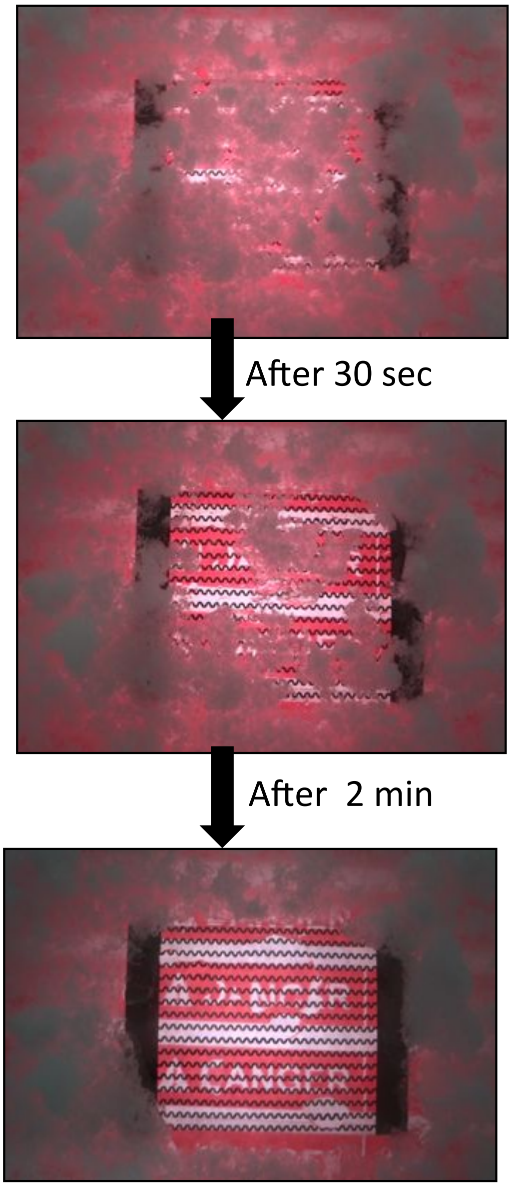

Fig. S9 Defrosting window is demonstrated using the zig zag patterned Ag electrode.

The patterned electrode (6 cm × 6 cm) is covered with the frost all around at the back side of Ag printed PET substrate. As soon as the voltage is applied, the frost starts disappearing at the patterned area where the heating takes place without affecting the frost at the remaining areas. The frost disappears completely within fraction of minutes with an applied voltage of 0.8 V (Fig. S9).

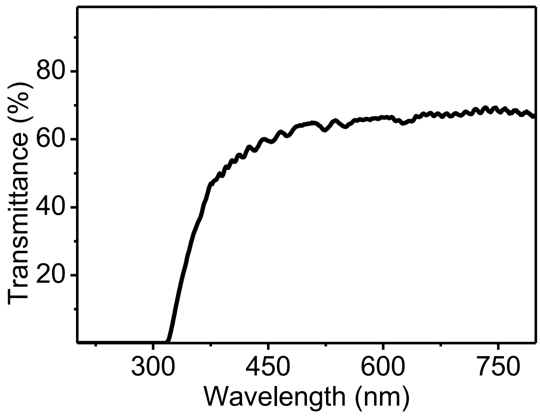

Fig. S10 Transmission spectrum from the substrate (2 layers of PET) and the encapulant (2 layers).

The combined transmission loss due to the substrate (2 layers of PET) and the encapulant (2 layers) stands at ~ 37% at 550 nm. This value was used for correcting the transmission values obtained from the device during switching.

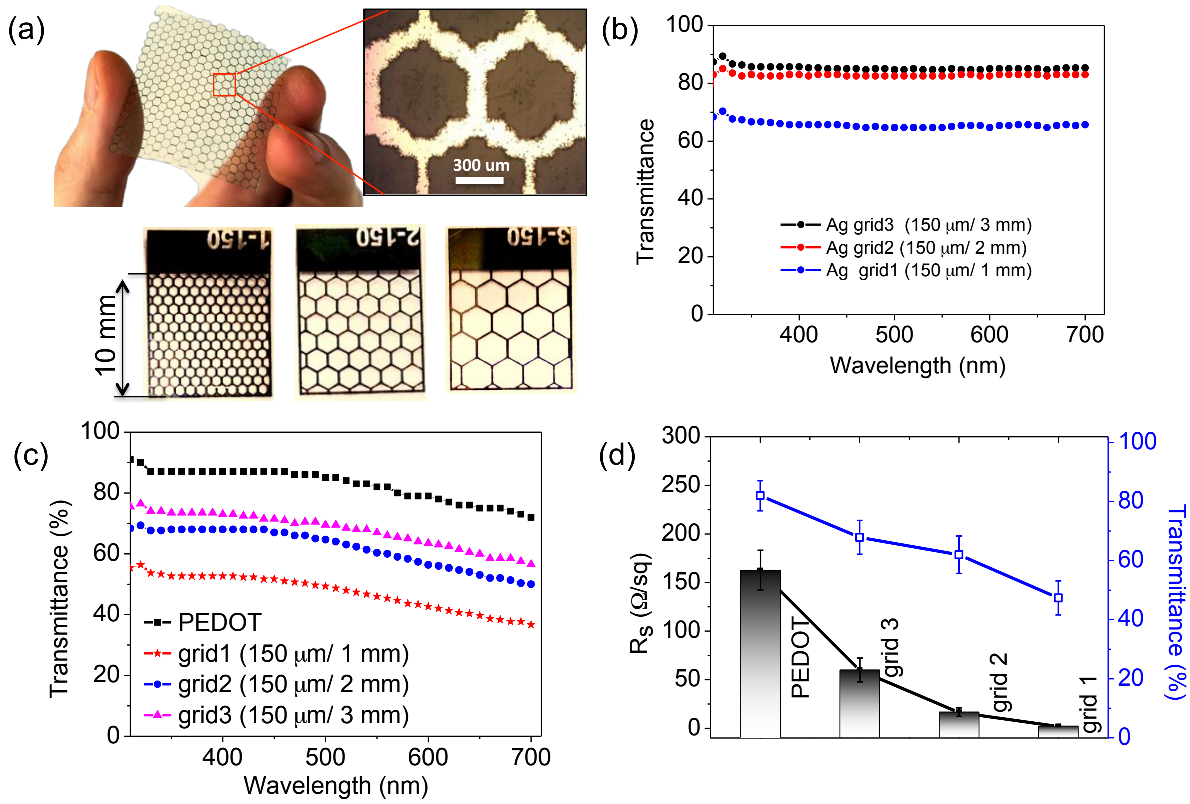

Fig. S11 Ag grids as transparent conducting electrode. (a) Photograph and optical microscope image (b) Transmittance spectra without and (c) with PEDOT and Ag grids of different hexagon grid size. The line width is kept 150 μm in all cases whereas the grid spacing is varied. (d) Plot of resistance and transmittance for grids coated with PEDOT as transparent conductors.

Table S4 A brief literature survey of hybrid Ag grid current collecting electrode and PEDOT.

*without PEDOT; # L- large area and S: small area

	Technique	Area (L/S)#	Grid Geometry	w (µm)	S (mm)	t (nm)	T (%)	Rs (Ω/sq)	PEDOT thickness (nm)	PCE (%)	Reference
1	ink-jet-printed Ag	L	Square	155	2	145	68.3	10.6	150	2.29	Semicond. Sci. Technol. 27(2012) 125002 (5pp)
2	Screen printed Ag	L	Hexagon	160	2-5	2000	92-93.6*	1*	100	1.82	Sol Energy Mater. & Sol. Cells 95 (2011) 1339–1343
3	Micromolding	S	Line pattern	20-40	0.1-0.8	100	85*	0.5*	160	1.0	Adv. Mater.2007,19, 2893–2897
4	grid embedded in PET	S	Hexagon	3	0.13	3000	85*	6.1	35	1.36	Sol. Energy Mater. & Sol. Cells 113 (2013) 85–89
5	Micro contact printing/wet etching	S	Square	5 10 20	0.05 0.1 0.2	30	78 80 82	9.1 146.3 254.1	220	3.21 2.93 2.85	Appl. Phys. Lett.96, 203301 (2010)
6	ink-jet printing	L	Hexagon	290	5	600	88.88*	4.83*	200	1.19	Sol Energy Mater. & Sol. Cells 104 (2012) 32–38
7	ink-jet, litho-graphic Mo/Al/Mo	L	Line pattern	325 180	2.5 2	600 120	87* 91*	2.46* 2.68*	100	1.4 1.47	Adv. Energy Mater. 2012, 2, 103–110
8.	thermal sintering Flash sintering	L	Hexagon	290 260	5	600 700	88.74 89.87	--	100	1.39 1.38	Org. Electronics 14 (2013) 38–46
9.	**Xerography**	**L**	**Hexagon**	**250**	**2**	**200**	**82**	**4**	**50**	**1.82**	**Present Study**

w is width of the electrode
S is spacing
t is thickness
T is transmittance
Rs is sheet resistance

Table S5 The optimized conditions for roll coating of solar cells

S.No	Layer	Concentration (mg/ml)	Temperature (°C)	Speed (m/min)	Flow Rate (ml/min)
1	Ag ink (TEC)	No dilution	60	0.6	0.2
2	PEDOT:PSS (PH1000)	10:3 in IPA	70	1	0.6
3	ZnO in acetone	40	60	2	0.2
4	P3HT:PCBM in 1,2-dichlorobenzene	40 (1:1)	60	1	0.2
Wetting of P3HT:PCBM layer with n-butanol to avoid dewetting of PEDOT					
5	PEDOT: PSS (PH5010)	1:1 in IPA	60	1	1.4
6	Ag (top electrode)	Flexographic printing			

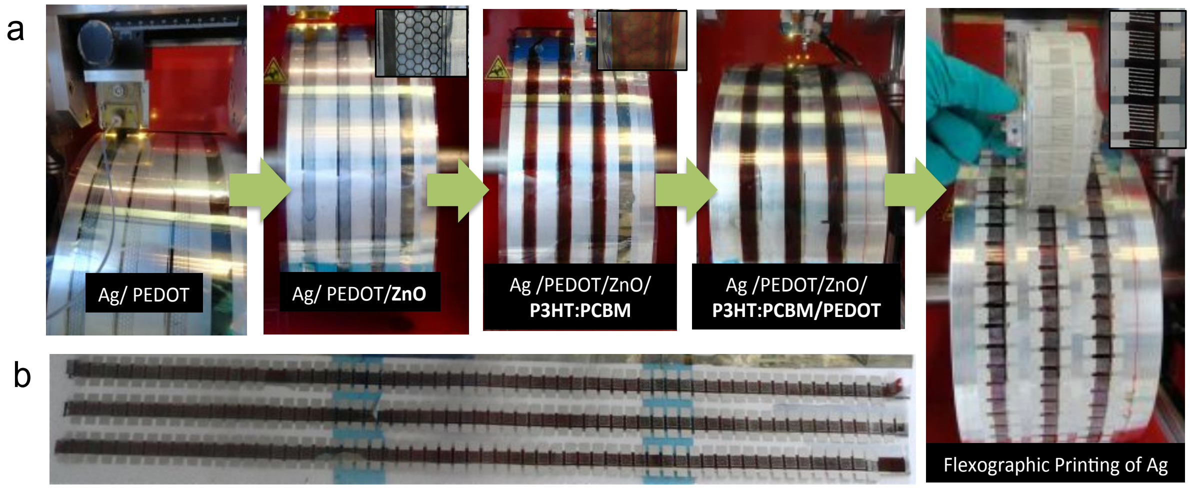

Fig. S12 (a) Photographs demonstrating the sequential steps for fabrication of solar cell. (b) Roll coated solar cells.